STAFF SUMMARY SHEET

	TO	ACTION	SIGNATURE (Surname), GRADE AND DATE		TO	ACTION	SIGNATURE (Surname), GRADE AND DATE
1	DFP	sig	*Timothy D Russell* O-5 1 AUG 2014	6			
2	DFER	approve	*Sozzi, AD22, 7 Aug 14*	7			
3	DFP	action		8			
4				9			
5				10			

SURNAME OF ACTION OFFICER AND GRADE	SYMBOL	PHONE	TYPIST'S INITIALS	SUSPENSE DATE
G. I. Font-Rodriguez, Professor	DFP	333-3276	XXX	

SUBJECT		DATE
Clearance for Material for Public Release USAFA-DF-PA- *396*		20140801

SUMMARY

1. PURPOSE. To provide security and policy review on the document at Tab 1 prior to release to the public.

2. BACKGROUND.
Authors: Dr. Gabriel Font-Rodriguez, DFP, x3276

Title: Computational Acceleration of Orbital Neutral Sensor Ionizer Simulation Through Phenomena Separation

Document type: Journal Article

Description: This paper describes numerical techniques for accelerating computations of plasma phenomena when large computational times are necessitated by the complexity of the physics.

Release Information: This document is being submitted for publication in the Journal of Computational Physics

Previous Clearance information: None

Recommended Distribution Statement: (Select one distribution statement from below and place on this line)
Distribution A, Approved for public release, distribution unlimited.

3. DISCUSSION. None

4. VIEWS OF OTHERS.   None

5. RECOMMENDATION. Sign coord block above indicating document is suitable for public release. Suitability is based solely on the document being unclassified, not jeopardizing DoD interests, and accurately portraying official policy.

// signed //

TIMOTHY D. RUSSELL, Lt Col, USAF
Deputy Department Head
Department of Physics

Tabs
1. Document

Computational acceleration of orbital neutral sensor ionizer simulation through phenomena separation

Gabriel I. Font[a]

[a]Dept. of Physics, US Air Force Academy, gabriel.font@usafa.edu

ABSTRACT

Simulation of orbital phenomena is often difficult because of the non-continuum nature of the flow, which forces the use of particle methods, and the disparate time scales, which make long run times necessary. In this work, the computational work load has been reduced by taking advantage of the low number of collisions between different species. This allows each population of particles to be brought into convergence separately using a time step size optimized for its particular motion. The converged populations are then brought together to simulate low probability phenomena, such as ionization or excitation, on much longer time scales. The result of this technique has the effect of reducing run times by a factor of $10^3 - 10^4$. The technique was applied to the simulation of a low earth orbit neutral species sensor with an ionizing element.

1. Introduction

The measurement of neutral species levels in the ionosphere has gained considerable importance due the effects of orbital ionospheric satellite drag. [1-4] Variation in orbital drag can change satellite trajectories and result in difficulties with ground-to-orbit communication. In addition, satellite motion and thruster firings can change the local orbital plasma environment leading to contamination and alteration of fields and the energies of particles surrounding the spacecraft.[5-8] Measurement of the neutral component of the ionosphere is usually carried out with some type of mass spectrometer. These instruments will typically first ionize the incoming flow and then measure the current to characterize the flux. Once the particles are ionized, electric fields can then be used to extract data about the particle energy, composition, or velocity distribution function.[9] In an effort to improve the design of an ionizer element for a neutral particle sensor, numerical simulation can be used to optimize the performance of the instrument. Simulation of these types of flow fields can be very difficult due to the non-Maxwellian nature of the velocity distribution functions, the non-continuum nature of the fluid, and the small ionization fractions involved. All of these problems lead to large computational workloads and long computational times. The present work details the strategies and techniques utilized in the acceleration of the numerical simulation of an ionizing element used in an orbital neutral particle sensor. The purpose of the study is to characterize the amount of current which can be expected from an ionizing element used by such a sensor.

Computation of neutral particle flows in orbit is difficult due to the non-continuum nature of the gas. A parameter often used to determine the expected level of continuum behavior is the Knudsen number, given by,

$$Kn = \frac{\lambda}{L}$$

(1)

where λ is the mean free path and L is the length scale of the flow. In low earth orbit, the mean free path is measured in thousands of meters.[10] For length scales comparable to a satellite, the Knudsen number, therefore, is greater than 10^3 and the flow is in a free-molecular regime. Therefore, it can not be treated with continuum (fluid) methods. For this reason, particle methods are typically employed in simulations of orbital neutral flows. In the present work, a Direct-Simulation-Monte-Carlo[11] (DSMC) technique is utilized to model particle collisions and a Particle-In-Cell[12] (PIC) technique is used to model the effects of electric and magnetic fields.

The computations will attempt to simulate the ionization process in an orbital neutral particle sensor. A schematic of the computational geometry is shown in Fig. 1.
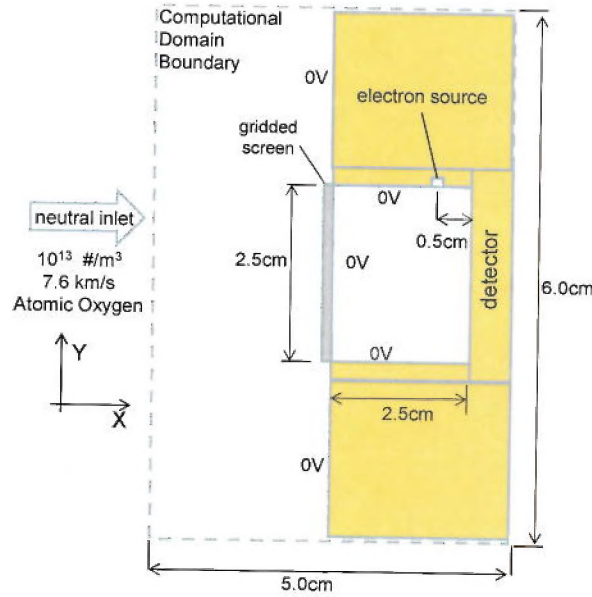

Fig. 1: Computational Geometry

The neutrals enter the computational domain on the left side. The density and velocity are set to be representative of flux of particles on the ram side of a satellite which is in an orbit with a 600km altitude. A portion of the neutrals will travel through a gridded grounding screen. For the present simulations, the screen is 100% transparent and serves only as a boundary condition for the electric potential. The screen and the walls of the ionization chamber are grounded to the spacecraft chassis. The voltage at the detector can be offset from ground as will be detailed below. Once the neutrals enter into the ionization chamber, they are bombarded by a beam of electrons from a source located on the top of the ionization chamber. The energy of the electrons is set to 100eV to match the peak of the ionization cross section for atomic oxygen, the dominant neutral in LEO. The resulting ions are then collected in the detector located on the right side of the ionization chamber. The computations treat the geometry in a 2-dimensional manner, although, the particles have 3-dimensional velocity distributions. The geometry is assumed to be

1cm in the direction normal to the page. The purpose of the study is to determine the amount of ions which can be expected to reach the sensor after being ionized by the electron beam.

2. Method

The simulation of the flow field detailed above is straight forward but is computationally very intensive. It requires modeling of three major physical phenomena: 1) the neutral flow and associated collisions, 2) the electron flow, 3) the ionizing collisions, and 4) the motion of the created ions. By inspecting each of these phenomena and dispensing with the components which do not affect the results in a statistically significant manner, the computational workload (run time) can be reduced by orders of magnitude.

We will first examine the neutral flow and associated collisions. The neutral flow will enter with a non-Maxwellian velocity distribution. For the purposes of this study, the neutral velocity distribution in the X (ram) and the Y and Z (perpendicular) directions will be as shown in Fig. 2. The X velocity distribution represents an orbital velocity flow of 7600m/s with a temperature of 2000K while the Y and Z velocity distributions represent a neutral population with a temperature of 1000K. Each distribution is essentially a 1D drifted Maxwellian, although the Y and Z components have no directed velocity. The different temperatures are chosen to be representative of a flow which may have been accelerated in an external electric field. In the computations, these velocity distribution functions (VDF) are sampled in order to generate the population of neutrals entering the computational domain.
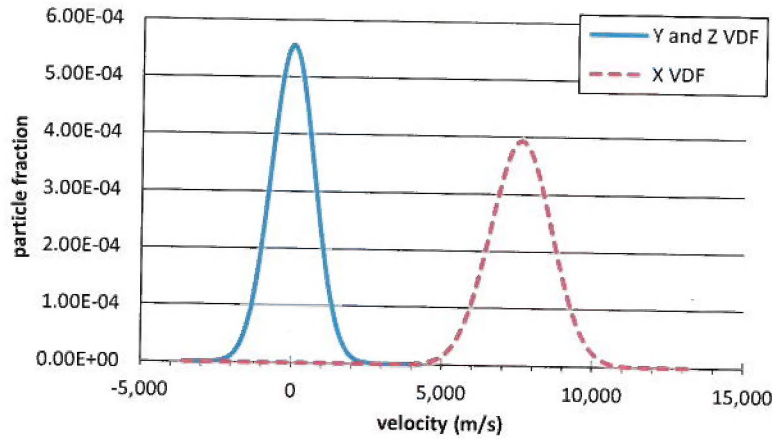

Fig. 2: Particle velocity distribution functions.

After entering the computational domain, the neutral particles can collide with other neutral particles. The average neutral collision frequency can be estimated with,

$$V_{col} = n_n \sigma V_{th} \tag{2}$$

Where n_n is the neutral density, σ is the collision cross section, and V_{th} is the thermal velocity. For the current conditions, the neutral-neutral collision frequency, v_{col}, is 0.015 s^{-1}. The transit time for the

neutrals through the computational domain (moving at orbital velocity of 7.6km/s) is only about 10^{-5} s. Therefore, the probability that a neutral collides with another neutral is of the order of 10^{-7} or only one in 10 million neutrals will suffer a collision. If the neutral-neutral collisions were to be ignored, it would only incur an error in the velocity distribution function of one part in 10^7. For this reason, neutral-neutral collisions will not be included in the computations. This will save the computational cost of calculating probabilities and pairing particles which must still be carried out even though no significant number of neutral-neutral collisions will take place. Neutral particles will still be allowed to collide with walls and suffer ionizing collisions with electrons but neutral-neutral collisions will not be calculated. Effectively, their velocity distribution functions will only be changed by wall collisions.

The second phenomena to be considered is the electron flow. This includes electron transport, electron-electron collisions, momentum transfer electron-neutral collisions, and electron-neutral ionizing collisions. Electron transport, the acceleration/deceleration and movement of electrons in ambient electric fields, is an important first order effect and will be retained in the computations. Electron-electron collisions, however, do not affect the electron velocity distribution function. This is because two colliding electrons have identical mass and the result of conserving momentum and energy is that the electrons simply exchange their velocity vectors. Therefore, there is no net effect on the electron population velocity distribution. For this reason, electron-electron collisions also will not be included in the computations.

Next, electron-neutral momentum transfer collisions will be considered. The electrons will enter the simulation at a rate of 0.1mA with an energy of 100eV and a temperature of 1000K. The average energy is chosen to match the peak of the atomic Oxygen electron impact ionization cross-section. At this energy, the average electron will be travelling with a velocity of 5.9×10^6 m/s and will cross the ionization chamber (2.5cm tall) in 4×10^{-9} s. Conservatively estimating the average elastic electron-neutral cross section to be of the order of $10^{-19} m^2$ and using eqn. 2 gives a collision frequency of about 6 per second. Since the electrons will only be in flight for 10^{-9} s, the probability of an electron suffering an elastic collision with a neutral particle is 10^{-8}, or one collision for every 100 million electrons. For this reason, the computations will also ignore electron-neutral momentum transfer collisions.

Next, electron impact ionization collisions will be considered. The atomic Oxygen electron impact ionization cross-section at 100eV, the average electron energy, is about $1.4 \times 10^{-20} m^2$. Again, using eqn. 2, this results in an average ionization collision frequency of $0.83 s^{-1}$. When coupled with the electron transit time, the average probability of ionization is 10^{-9}. This presents a tremendous computational problem: on average, 10^9 electrons must be simulated for every ionization event that takes place. This is exceedingly small. However, this phenomena can not be ignored since determining the amount of ionization is the principal goal of the study.

The present ionizer will use an electron current of 0.1mA. This represents 10^{14} electrons per second which would produce 10^6 ions/sec using the above stated probability. In order to take statistics on 10^4 ions, a total simulation time of 10^{-2} seconds is needed. Since the electrons are travelling at 10^6m/s and the cell size is of the order of 10^{-3}m, the electrons will be limited to time step of the order of $10^{-9} - 10^{-10}$s. Therefore, in order to simulate a total of 10^{-2}s, a total of 10^8 time steps are needed. This represents an unacceptable computational work load. Parallelization of the computer code will not alleviate this

problem since the flow will be evolving in time and must be computed in chronological order. Clearly, a different computational strategy is needed.

We can take advantage of the physics of the current problem in order to decrease the work load by noting the influence that each phenomena has on the others. As explained above, because electron-neutral momentum transfer collisions are so infrequent, the neutral particle velocity distribution function is largely independent of the electron population by a factor of better than one part in 10^8. This suggests that the neutral population in the computational domain can be simulated independent of the electrons. This would allow the neutrals to be brought to equilibrium using a time step that is consistent with the neutrals and not restricted by the high velocity of the electrons. For the current conditions, the neutral time step is determined by the orbital velocity (7600m/s) and the cell size (10^{-3}m) and is of the order of 10^{-7}s, a 1000 fold speed up over the simulation which includes electrons. Similarly, since the electron distribution is independent of the neutrals, their equilibrium condition can be computed without having to compute neutral motion. After independent convergence to equilibrium, the neutral and electron populations, with the imbedded velocity distribution information, can be saved and used as input to a simulation involving only the ionization and transport of the ions. If the ion population remains small in comparison to the electron population, the interaction between the two need not be computed. This final simulation would, therefore, not need to compute any changes to the neutral or electron populations. This can not be determined a priori, but will turn out to be the case as will be shown below.

In order to improve statistics and further reduce run times, one further modification is proposed. Since the time step will need to be as small as 10^{-7}s in order to follow the ion motion, an ionization rate of 10^6 per second will not produce many ions during each time step. Since statistical significance increases with the number of computational particles in the simulation, more ion particle creation during each time step is desired. This can be achieved by allowing the creation of fractional ions or computational particles that represent only a fraction of an ion. This will be accomplished in the following manner: The precomputed neutral and electron populations will be used to determine the total ionization rate in each cell. During each time step, a single particle representing a fraction of an ion will be generated in each cell. The velocity of the ion will be determined by carrying out a collision between a randomly chosen neutral and electron particle. The weighting of the particle, however, will be set to the number (or fraction) of ions which statistically should be generated in each cell during each time step. Therefore, instead of waiting an average of 10 – 10,000 time steps for each new ion, ions will be generated during each and every time step and their population and behavior will be determined in a fractionally weighted manner. Fractional particles will not change the physics since the density will be low enough to preclude significant numbers of collisions. In effect, the scheme remains unchanged from where a single computational particle represented multiple real particles. This strategy will generate more computational ion particles but the same average number of real physical particles. Therefore the statistics will be improved and the required run times will be reduced.

The effect on the electron population still needs to be determined. If the ion density magnitude approaches the electron density magnitude, the electric fields will begin to be cancelled and the electron flow will need to be recomputed. The ion density will be increased by the ionization events and decreased by the neutralization at the walls. The ion flow velocity will start near the neutral orbital velocity (because the ions are born with the velocity of the parent neutral) and then may change as the

ions are accelerated by local fields. Therefore, there is no way to determine the final ion density a priori. Computations, which will be shown below, indicate that the ion density never rises above 10^7 - $10^8 m^{-3}$. Comparing this to the average electron density ($10^{12} m^{-3}$) shows that there will exist $10^4 - 10^5$ electrons for every ion. Therefore, they will not significantly change the potential distribution inside the ionization chamber and the effect on the electrons will not be significant. In addition, the low density of the ions results in a very small collision frequency between them and the neutrals ($v_{col} = 0.006$ s^{-1}). During the transport to the walls (about 10^{-6}s at near orbital velocity), the probability of an ion suffering a collision is of the order of 10^{-9}. Therefore, since only one particle in 10^9 will suffer a collision, the ion flow will not impact the neutral distribution either and can be computed independently of both the electron and neutral particle distributions.

In summary, because of the low collisionality between neutrals and electrons, each will be computed separately and using a time step optimized to its motion. The converged populations will then be frozen and used in the ionization source terms. This will allow computation of the low-probability ionization events over long time periods without the necessity of computing the neutral and electron motion. Because of the low collisionality between the ions and the neutrals, the resulting ion flow will also be computed separately. In order to improve statistics and further reduce run times, fractional ion generation is employed which reproduces the statistical ionization rate. The result of these techniques is a reduction in the number of time steps necessary to reach convergence from 10^8 to a number less than 10^5. This has the effect of reducing the run times by a factor of $10^3 - 10^4$.

3. Results

The computations are initiated using the geometry detailed in Fig. 1. The computational grid is formed by cells which are 1mm long (X) by 1mm tall (Y) by 10mm into the page (Z). This represents a cell size many orders of magnitude smaller than the mean free path ($>10^3$ m) and smaller than the Debye length (~ 0.004 m). Note that the Debye length is strictly not applicable in the current simulations because the flow is not a true plasma since it is never quasi-neutral. Therefore, it never exhibits the shielding behavior of an actual plasma. Never-the-less, the cell size is kept small in order to maintain sufficient accuracy in modeling of the geometry. The computations are treated as two dimensional although the particles have velocities in the three dimensions. Particles leaving the domain in the Z direction (into the page) simply reenter the domain from the opposite side maintaining the same Z velocity. Particles striking walls are either reflected in a diffuse or specular manner. With diffuse reflection, the particles striking the wall leave with direction to the wall that has a cosine probability distribution. The average velocity is determined by the wall temperature (full accommodation) which is set to 300 K. With, specular reflection, the particles leave the wall with the same angle to the normal as they had on impact. All neutrals enter the simulation from the left side of the domain with a velocity distribution given by Fig. 2. The velocity distribution is further modified such that the x and y velocities are rotated 10deg. This simulates a sensor that is pointed in a direction that is not exactly into the RAM. Computations are continued for several hundred neutral flight times which allows the number of particles

in the domain to stabilize. The resulting neutral density contours for diffuse and specular wall reflection are displayed in Fig. 3.
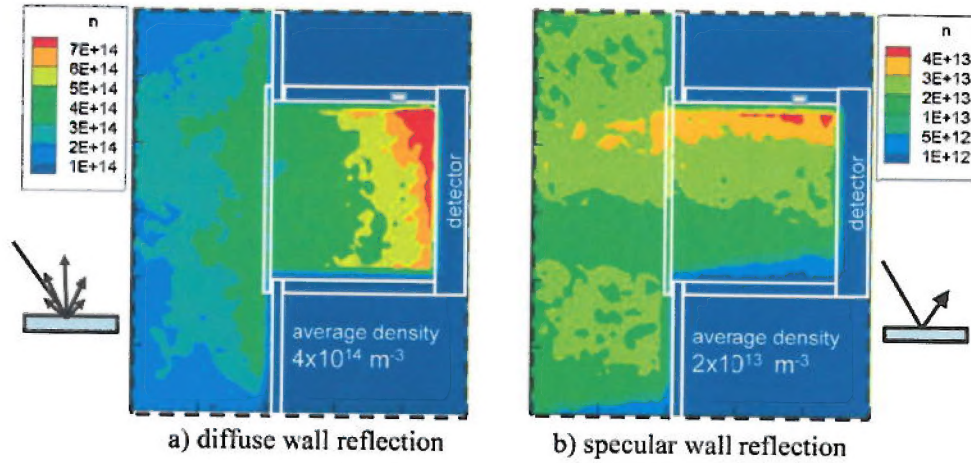

a) diffuse wall reflection   b) specular wall reflection

Fig. 3: Neutral number density contours (m^{-3}) for diffuse and specular wall reflection cases. The ambient entry density is $1 \times 10^{13} m^{-3}$ with the flow entering at an angle 10deg. upward.

Computations show that the result of the neutrals entering with a velocity angled upward by 10 deg. is a neutral pile up near the top of the ionization chamber, especially for the specular reflection case. The computations also show that diffuse reflection results in higher density levels in the ionization chamber of the sensor. The average density for the diffuse reflection case is 40 times the ambient density, whereas for specular reflection, it is only a factor of 2 times the ambient density. This occurs because, with diffuse reflection and full accommodation, the particles leave the wall with a much smaller velocity (wall thermal vs orbital or 700m/s vs 7600m/s) since their energy is set to equal the wall temperature. Ref. 13 suggests that at LEO, diffuse reflection may be a more appropriate model, while at higher altitudes such as GEO, specular reflection may dominate. In order to make a conservative estimate of the lowest number of ions impacting the detector, this study will use the specular reflection model and the resulting lower levels of neutral density.

The electron flow was simulated independently of the neutral flow because of the low number of collisions taking place between the two, as detailed in the previous section. The electric potential was solved at each time step and the electric field forces were applied to the electron particles as they moved through the domain. All walls were held at a 0 voltage boundary condition. Electrons impacting the walls were removed from the computation because the walls were modeled as being made of a conducting material. No secondary electron emission is currently modeled. Three electron current levels were simulated: 0.01, 0.1, and 1mA. The resulting electron number density contours are show in Fig. 4.
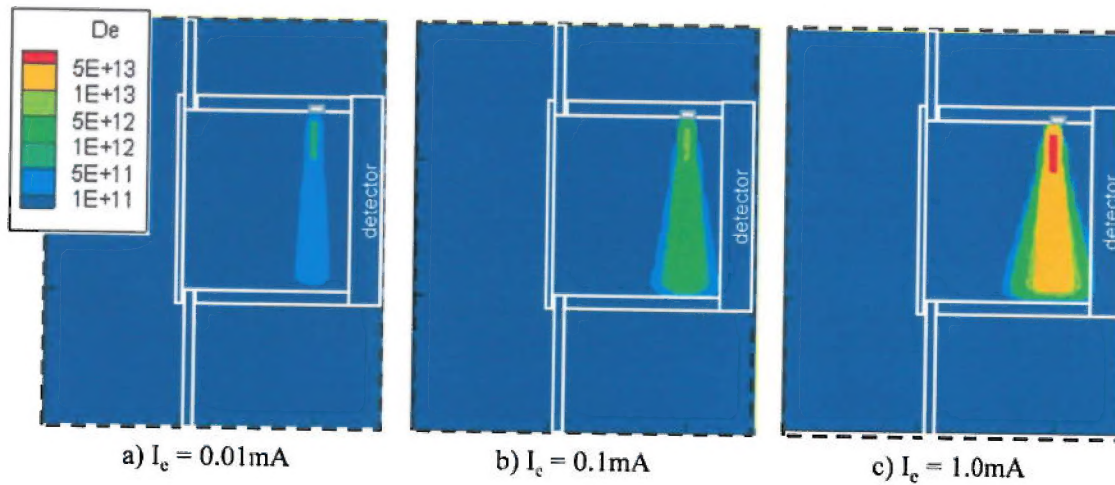
Fig. 4: Electron number density contours (m⁻³) for different electron current levels.

As the electron current increases from 0.01 – 1.0 mA, the average electron number density increases linearly from 10^{11} – 10^{13} m⁻³. The electron beam width also increases with increasing current levels and in the case where the current reaches 1.0 mA, the electron beam clearly is impinging on the detector. This anomalous electron flux may alter the measured current at the detector. Current contamination could be avoided by simply moving the electron emitter to a position farther from the detector or biasing the detector face. The reason for the beam broadening can be found in the electric potential contours shown in Fig. 5.
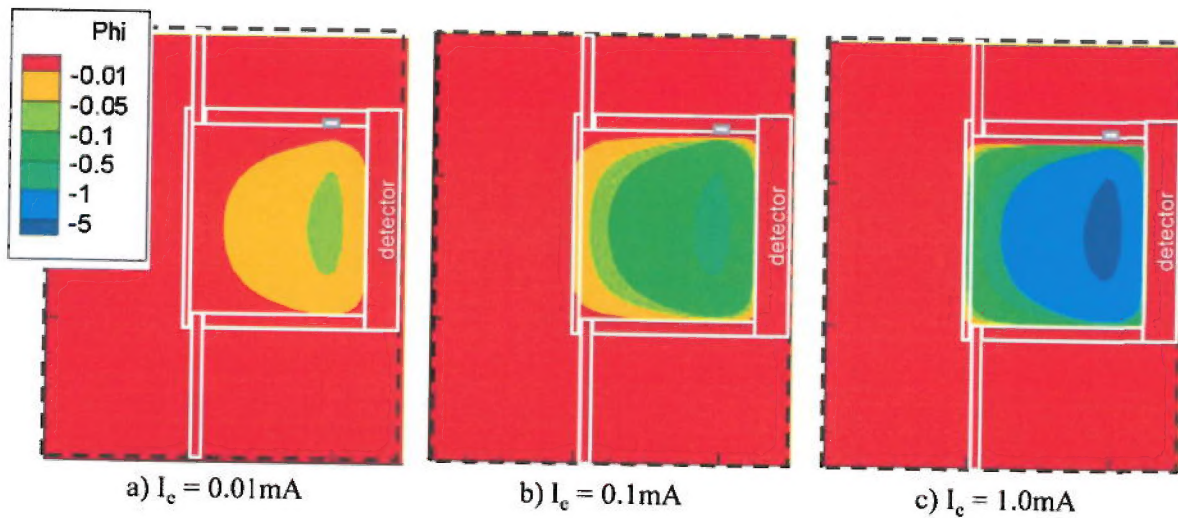

Fig. 5: Electric potential contours (V) for different electron current levels.

Fig. 5 shows that the presence of the electron beam creates a negative potential region in the ionization chamber. The level of negative potential increases as the electron current increases, from about -0.05 V for a current of 0.01mA to -5 V at an electron current level of 1.0mA. The negative potential well creates electric fields that spread the electron beam. This negative potential well also creates another problem: ions born inside it must have sufficient energy to climb out and reach the detector. For the

present case, the atomic oxygen neutrals enter with an energy of 4.6eV due to the 7600m/s entry speed. Since the bulk of the energy of ionization will be carried away by the liberated electron, ions will be born with an energy close to that of the neutrals. An ion with less than 5eV will not be able to reach the detector if it is born at the center of the potential well created by the presence of the electron beam.

The neutral and electron particle populations computed above were then used to calculate ionization rates in a simulation of the ions. Neutral and electron particles were chosen at random in each cell in order to preserve the collisional dynamics of the electron impact collisions and the resulting ions were allowed to move under the influence of the local electric fields. The resulting ion number density contours are shown in Fig. 6.
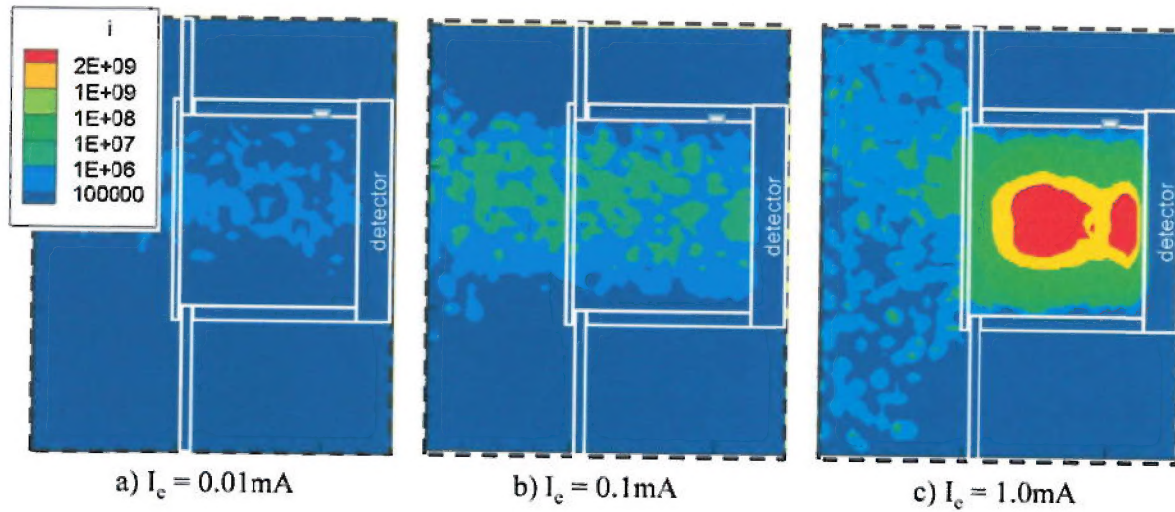

a) $I_e = 0.01$mA   b) $I_e = 0.1$mA   c) $I_e = 1.0$mA

Fig. 6: Ion number density contours (m^{-3}) for different electron current levels.

The results show that the average ion density increases, as expected, with increasing electron current. In each case, ions are noted to exit the ionizing chamber. This flux of ions is due to ions created from neutrals that had already rebounded from the detector face and had a velocity pointed outward from the detector. For the two lowest electron current levels, the ion density increases linearly with electron current. For the last case ($I_e = 1.0$mA), however, the ion density increases more than can be attributed to the increased electron current alone. In this case, the negative potential well (Fig. 5c) is of the same order as the neutral energy. This results in a dynamic situation where a large portion of the ions inside the ionization chamber are trapped due to their inability to climb out of the potential well. These ions would presumably be released and be free to impact the detector or leave the ionizing chamber once the electron current was turned off and the resultant potential well no longer existed. Therefore, operating the sensor at high electron current levels can create situations where a significant portion of the created ions can not reach the detector.

The problem of ion trapping can be mitigated by biasing the detector face. For example, if the detector in the 1.0mA case were to be biased to a level higher than the value of the potential well, a path would be created where the ions can escape and reach the detector. This was attempted by biasing the detector face to -15V and repeating the computations. The resulting electric fields did not affect the

neutral flow, therefore, it was unnecessary to recalculate them. The bias was applied and the electrons and ions were recalculated. The results are shown in Fig. 7.

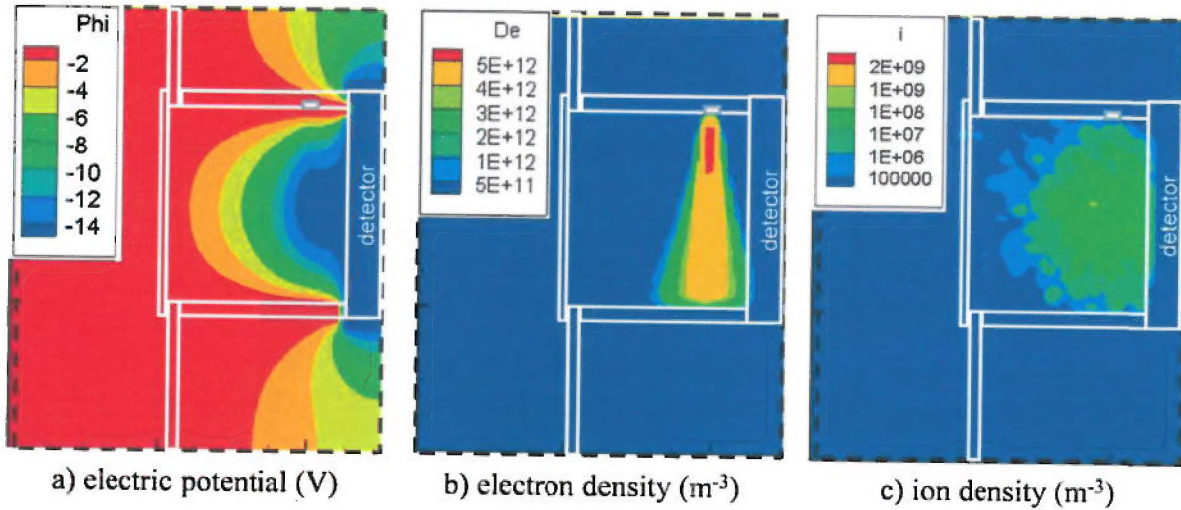a) electric potential (V)   b) electron density (m⁻³)   c) ion density (m⁻³)

Fig. 7: Effects on electric potential, electron density, and ion density of biasing the detector face.

Figure 7a shows the electric potential inside the ionization chamber when the detector face is biased to -15V and a current of 1mA is used. There is now a zero voltage potential difference between the center of the ionization region and the detector. This allows all of the created ions to reach the detector. The electron density distribution, shown in Fig. 7b, shows more spreading than exhibited in Fig. 4c. This is due to the electric fields (potential gradient) created by the biased detector. The average ion density, shown in Fig. 7c, now reaches only $10^7 m^{-3}$ which continues the linear variation with electron current exhibited by the 0.01 and 0.1mA cases. This indicates that ions are no longer being trapped. In fact, the lack of ions outside of the ionization chamber in Fig. 7c, suggest that even the ions born with velocities which would normally take them out of the chamber are now largely being attracted to the detector. The ion impacts to the detector are shown in Fig. 8. At low electron currents, 0.01 and 0.1mA, the potential well created is smaller than the ion energy and biasing the detector does not affect the ion current to the detector. At an electron current of 1mA, however, biasing the detector face is necessary to collect all of the created ions and avoid ion trapping.
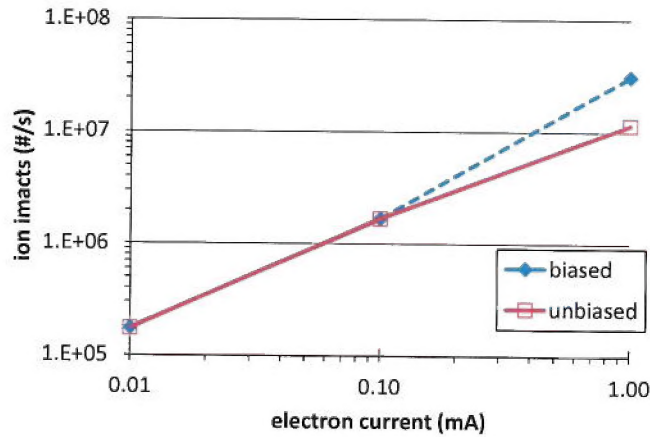
Fig. 8: Effects of detector bias on the number of ion impacts at the detector.

4. Conclusions

Simulation of orbital phenomena is often difficult because of the non-continuum and non-Maxwellian nature of the flow, which forces the use of particle methods, and the disparate time scales from low probability phenomena, which make long run times necessary. In this work, the computational work load has been reduced by taking advantage of the low number of collisions between different species. This allows each population of particles to be brought into convergence separately using a time step size optimized for its particular motion. The converged populations can then be brought together to simulate low probability phenomena on much longer time scales. The result of this technique has the effect of reducing run times by a factor of $10^3 - 10^4$. The technique was applied to the simulation of a low earth orbit neutral species sensor with an ionizing element. The simulations demonstrate the viability of such a sensor and reveal the need for detector face bias when large ionizing currents are used.

References

[1] M. F. Storz, B. R. Bowman, J. I. Branson, S. J. Casali, and W. K. Tobiska, High Accuracy Satellite Drag Model (HASDM), Advances in Space Research, 36(12) (2005) 2497-2505.
[2] J. F. Liu, R. G. France, and H. B. Wackernagel, An Analysis of the Use of Empirical Atmospheric Density Models in Orbital Mechanics, AAS/AIAA Astrodynamics Specialist Conference, (1983).
[3] F. A. Marcos, Accuracy of Atmosphere Drag Models at Low Satellite Altitudes, Adv. Space Research, 10(3) (1990) 417-422.
[4] Nicholas, T. Finne, I. Galysh, M. Davis, and L. Healy, The Atmospheric Neutral Density Experiment (ANDE), 2009 NRL Review (2009) 138-142.

[5] E. Wulf and U. vonZahn , The shuttle environment: Effects of thruster firings on gas density and composition in the payload bay, J. Geophys. Res., 91(A3), (1986) 3270–3278, doi:10.1029/JA091iA03p03270.

[6] J. S. Machuzak, W. J. Burke, J. M. Retterer, D. E. Hunton, J. R. Jasperse, and M. Smiddy, Effects of thruster firings on the shuttle's plasma and electric field environment, J. Geophys. Res., 98(A2) (1993) 1513–1530, doi:10.1029/92JA02041.

[7] U. Samir, N. H. Stone, K. H. Wright Jr., On plasma disturbances caused by the motion of the space shuttle and small satellites: A comparison of in situ observations, J. Geophys. Res., 91 (1986) 277–285.

[8] U. Samir, and G. L. Wrenn, Expermental Evidence of an Electron Temperature Enhancement in the Wake of an Ionospheric Satellite, Planet. Space Sci., 20 (1972) 899-904.

[9] C. Enloe, K. Habush, R. Haaland, T. Patterson, C. Richardson, C. Lazidis, and R. Whiting, Miniaturized electrostatic analyzer manufactured using photolithographic etching, Rev. Sci. Instrum., 74(3) (2003) 1192–1195.

[10] D. Hastings, and H. Garrett, Spacecraft-Environment Interactions, Cambridge University Press, Cambridge, 1996.

[11] G. Bird, Molecular Gas Dynamics and the Direct Simulation of Gas Flows, Oxford University Press, Oxford, 1994.

[12] C. Birdsall, and A. Langdon , Plasma Physics via Computer Simulation, Taylor and Francis, New York, 2004.

[13] K. Moe, and M. M. Moe, Gas-surface interactions and satellite drag coefficients, Planet. Space Sci., 53 (2005) 793-801. DOI: 10.1016/j.pss.2005.03.005